Ginzburg-Landau theory of vortices in superfluid ^{3}He-B

E. V. Thuneberg

Materials Science Center, Clark Hall, Cornell University, Ithaca, New York 14853

(Received 24 February 1987)

Vortices in superfluid ^{3}He differ qualitatively from all other vortices. In conventional quantized vortices (^{4}He, superconductors) the order parameter is a scalar function with cylindrical symmetry that vanishes on its axis, but in superfluid ^{3}He the order parameter has nine complex components. More interestingly, the symmetries of the differential equation describing the vortices can be broken by its solutions. In the pressure-temperature phase diagram of ^{3}He-B, there is a first-order transition (observed in the shift of the NMR line) between two different vortices that, as recent theory has shown, have different broken symmetries. The vortex observed at high pressures has broken parity with either left- or right-handed vortices. The low-pressure vortex (which is the vortex obtained in the weak-coupling Bardeen-Cooper-Schrieffer theory) has, in addition, broken rotational symmetry around its axis, resulting in a novel double-core structure. The Ginzburg-Landau theory of vortices reproduces the properties of the transition, accounts well for the measured susceptibility and magnetization, and gives detailed predictions about properties not yet measured, such as the jump of the magnetization in the transition, the shift of the transition line in magnetic field, and the orientation of the double-core vortex. The lack of helical instability in the double-core vortex implies that the identification of the vortices is unique. The transition between vortices is interpreted in simple physical terms. A qualitative explanation is given to the metastable state of the low-pressure vortex observed at low temperatures. The numerical method for solving the Ginzburg-Landau equation is discussed.

I. INTRODUCTION

Superfluids cannot rotate as a solid body. Instead, the rotational state is realized by an array of quantized vortex lines in the fluid. While these vortices have been extensively studied in the familiar superfluid ^{4}He, this paper deals with the other superfluid isotope, ^{3}He, where vortex experiments have been carried out since 1981. More specifically, the vortices are studied in the B phase of ^{3}He. This phase was considered as roughly equivalent to the ^{4}He superfluid phase until the remarkable observation of a transition line within the B-phase region[1–4] (see Fig. 1). Interpreting this as a transition between two different kinds of quantized vortex lines means that the vortex structure in ^{3}He-B must be more complicated than in ^{4}He, where only one kind of vortex is possible. It was a challenge for theory to explain the transition and describe the two vortices.

All the theoretical studies of vortices in ^{3}He-B have used the Ginzburg-Landau (GL) theory. The GL differential equations were first correctly solved by Ohmi, Tsuneto, and Fujita.[7] I call their solution the normal-core vortex. They noted that the vortex has a small magnetization at zero field. A second type of vortex was found by Salomaa and Volovik.[8,9] I call it the A-phase-core vortex. (Salomaa and Volovik originally named it the v vortex according to their symmetry analysis. Because the vortices are now identified, I prefer the more easily understandable name. Also, there is a large number of symmetry classes that could have the name nonaxisymmetric v vortex they use for the double-core vortex.) They also applied the standard symmetry analysis[10] to vortices and obtained a useful,

partial classification of the possible symmetries of vortices. They interpreted the vortex observed at low pressures as the A-phase-core vortex, but they were unable to identify the high-pressure vortex: they found the normal-core vortex to be only a saddle point of energy.
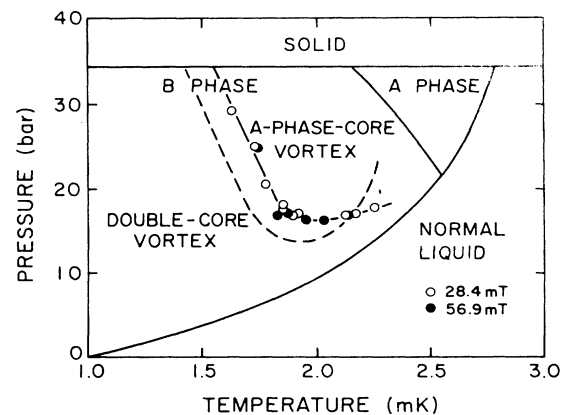
FIG. 1. The phase diagram of superfluid ^{3}He in the temperature-pressure plane. In addition to the superfluid A and B phases, the figure shows the vortex-core transition (solid line with data points) observed by NMR in rotating B phase (according to Ref. 4). The line curves upwards when approaching the superfluid transition line but the NMR signal goes small there and the point where the lines meet is not accurately known. The dashed line is another transition line observed in the critical velocity in 20-μm powder (Ref. 5) at zero field ("hydrodynamic experiment"). This transition is not considered in this paper, except for a couple of remarks; see Ref. 6 for a theoretical discussion of it.

This result was reproduced by Passvogel, Schopohl, and Tewordt[11] and by Hasegawa.[12] Fetter and Theodorakis[13,14] made a variational ansatz and found a transition between the normal-core and A-phase-core vortices. It was not immediately clear whether their apparent disagreement with Ref. 8 was caused by their more accurate input parameters (β parameters) (Ref. 15) or by their less accurate solution of the GL equation. This puzzle was resolved when a third vortex was found.[16] This double-core vortex has broken rotational symmetry around the vortex axis. The low-pressure vortex was identified as the double-core vortex and the high-pressure vortex as the A-phase-core vortex. Shortly afterwards, Salomaa and Volovik[17] confirmed the existence of the double-core vortex in the weak-coupling region by their variational ansatz.[18]

In this paper I will discuss the theory of isolated vortices in ^{3}He-B as completely as possible within the GL theory. This means describing the equilibrium properties in the neighborhood of the superfluid transition temperature $T_c(p)$. I will describe the order parameters of the vortices and calculate the energies. It will be demonstrated that many of the properties of the vortices can be understood in simple terms of bulk phases and their interfaces. It is argued that the present identification of the vortices is unique. I will derive the parameters through which the vortices affect the $\hat{n}$ texture, which is the long-wavelength soft mode of ^{3}He-B. I will not go into the determination of the $\hat{n}$ texture and the NMR signal in specific geometries, but that can straightforwardly be done using the standard texture theory[19] and the parameters given here. It is of interest to study the orientation of the double-core vortex in the plane perpendicular to its axis. It turns out that this is determined by the dipole interaction up to fields as high as 50 mT. The shift of the transition line in magnetic field is calculated as a function of the $\hat{n}$ vector and from the experimental transition line in the p-T plane at 28.4 mT the shape of the line at zero field is estimated. A comparison between theory and experiment is given concerning susceptibility, magnetization, and properties of the transition. A qualitative explanation is given to the metastable state of the low-pressure vortex observed at low temperatures.

In Sec. II the standard GL theory is reviewed with special emphasis on the numerical values of the input parameters. The mathematical formulation of the vortex problem is derived in the following section. The different vortex solutions are discussed in Secs. IV and V, and the numerical method is explained in Sec. VI. Section VII deals with the interaction of the vortices with the $\hat{n}$ texture and the magnetic field. Finally, a comparison with experiments is made in Sec. VIII. This article tries to be selfcontained. For the matters not covered here (such as introduction to vortices in ^{4}He or the theory of vortices in the A phase, for example) I should refer to several review articles.[20−22]

II. GINZBURG-LANDAU THEORY

Between superfluid ^{4}He and ^{3}He, there is one crucial difference relevant for this paper: In the Bose system (^{4}He) there is no reliable microscopic theory or any theory that goes beyond hydrodynamic theories. In contrast, in ^{3}He there is the quasiclassical theory, which can perhaps be considered as the most successful theory of condensed-matter physics. The quasiclassical theory contains the Landau Fermi-liquid theory and the Bardeen-Cooper-Schrieffer (BCS) theory of superconductivity as special cases. The quasiclassical theory is an exact expansion in the small parameter $T_c/T_F \approx 10^{-3}$ (the superfluid transition temperature divided by the Fermi temperature). Its results should be very accurate and they can be obtained with reasonable amounts of computation. One should be able to explain almost all measurements in superfluid ^{3}He theoretically using this theory. A review of the quasiclassical theory as it applies to ^{3}He is given in Ref. 23.

Liquid crystals exhibit properties that are often compared with superfluids. From the point of the discussion above, they belong to the same category as ^{4}He because they lack a reliable microscopic theory.

The mathematical complexity of the general quasiclassical theory can be reduced by restricting the temperature to the neighborhood of the superfluid transition temperature T_c. The general theory reduces to the Ginzburg-Landau (GL) theory in this temperature range, which is called the GL region. The GL theory is not considered as a phenomenological theory here but rather a special case of the quasiclassical theory. For the purpose of identification of the two vortices, we know a $priori$ that the GL theory should give the answer (supposing that the transition line goes into the GL region, which the experiments seem to support). In ^{4}He there is no justified GL theory and a transition of this kind would be much more difficult to understand there.

The extent of the GL region depends on the property one is interested in. The GL theory usually gives accurate results down to temperatures $\approx 0.5T_c$ in ordinary superconductors. In ^{3}He-B the region of validity is reduced mainly because there are several possible states which have small energy differences. For example, the GL theory can predict the points where the A-B and the vortex-core-transition lines meet the superfluid-transition line (Fig. 1) but it cannot say anything about the slopes of the lines. For a given state, the GL theory should be effective also below T_c but the validity region is probably not as big as in superconductors because of the large Fermi-liquid corrections. An example of this is the critical velocity shown in Fig. 4 of Ref. 24. It is well known that the quasiclassical (and GL) theory is valid essentially up to T_c because the critical fluctuation region is vanishingly small in ^{3}He.

For completeness, I will review the standard GL theory below. Several input parameters appear in the theory and the comparison with experiment depends strongly on their values. Therefore, they are calculated from cutoff-independent formulas only and the strong-coupling corrections are included whenever they are known. The numerical values of the parameters are listed in Table I at three different pressures.

The main contributions to the free-energy functional are the bulk energy[32,33]

$$F_b = \int d^3r \{ -\alpha \operatorname{Tr}(\underline{A}\ \underline{A}^{T*}) + \beta_1 |\operatorname{Tr}(\underline{A}\ \underline{A}^T)|^2$$

$$+\beta_2[\operatorname{Tr}(\underline{A}\ \underline{A}^{T*})]^2 + \beta_3 \operatorname{Tr}(\underline{A}\ \underline{A}^T \underline{A}^* \underline{A}^{T*})$$

$$+\beta_4 \operatorname{Tr}(\underline{A}\ \underline{A}^{T*}\underline{A}\ \underline{A}^{T*})$$

$$+\beta_5 \operatorname{Tr}(\underline{A}\ \underline{A}^{T*}\underline{A}^* \underline{A}^T) \} \tag{1}$$

and the kinetic (or gradient) energy

$$F_k = K \int d^3r [(\gamma - 2)\partial_i A_{\mu i}\partial_j A_{\mu j}^*$$

$$+\partial_i A_{\mu j}\partial_i A_{\mu j}^* + \partial_i A_{\mu j}\partial_j A_{\mu i}^*] \ . \tag{2}$$

Here $\underline{A}$ is the order parameter which is a complex 3×3 matrix. The components of $\underline{A}$ are denoted by $A_{\mu i}$, where μ is the coordinate index in spin space and i in the orbital space. The rectangular coordinates x, y, and z are used for μ and i throughout this paper. $\underline{A}^T$ denotes the transpose matrix of $\underline{A}$, and $\underline{A}^*$ the complex conjugate of $\underline{A}$.

The parameter α in (1) is equal to $N(0)(1 - T/T_c)/3$ because the strong-coupling corrections are negligible[27] $[N(0) = m^*k_F/2\pi^2\hbar^2]$. For the β_i's the weak-coupling (WC) quasiclassical theory gives

$$-2\beta_1^{WC} = \beta_2^{WC} = \beta_3^{WC} = \beta_4^{WC} = -\beta_5^{WC}$$

$$= \frac{7\zeta(3)}{120\pi^2}N(0)\frac{1}{(k_B T_c)^2} \tag{3}$$

which are inadequate to describe superfluid ^{3}He. Strong-coupling corrections give a nontrivial pressure dependence to the β parameters. There are various proposals for modeling the pressure dependence; see Ref. 15 for a discussion. The numerical studies of this paper use the Sauls-Serene values,[27] which are deduced from normal-state data and from $T_c(p)$. These give the tricritical point at the pressure of 28.5 bars which does not differ too much from the true pressure (21 bars). The lowest pressure where the parameters are listed in Ref. 27 is 12 bars and the weak-coupling values are used at zero pressure in this paper. The gradient energy coefficients are

$$K = \frac{7\zeta(3)}{240}N(0)\left[\frac{\hbar v_F}{\pi k_B T_c}\right]^2 \tag{4}$$

and $\gamma = 3$ in the weak-coupling theory. These are used in the numerical calculations at all pressures because the strong-coupling corrections are estimated only at the melting pressure.[34]

In addition to the terms (1) and (2), there are energy

terms which in general are much smaller. The dipole energy, which couples the spin and orbital directions, is

$$F_D = g_D \int d^3r [\ |\operatorname{Tr}(\underline{A})|^2 + \operatorname{Tr}(\underline{A}\ \underline{A}^*) - \tfrac{2}{3}\operatorname{Tr}(\underline{A}\ \underline{A}^{T*})] \ . \tag{5}$$

There are two magnetic field terms. The first term, which is quadratic in $\mathbf{H}$, is

$$F_Z = g_Z \int d^3r\ \mathbf{H}\cdot\underline{A}\ \underline{A}^{T*}\cdot\mathbf{H} \ , \tag{6}$$

which defines the susceptibility $\underline{\chi}$ through $F_Z = -\mathbf{H}\cdot(\underline{\chi} - \underline{\chi}^n)\cdot\mathbf{H}/2$, where $\underline{\chi}^n$ is the susceptibility of normal Fermi liquid. The second magnetic field term is linear in $\mathbf{H}$:

$$F_Z' = g_Z' \int d^3r\ i\epsilon_{\kappa\mu\nu}H_\kappa A_{\mu i}A_{\nu i}^* \ , \tag{7}$$

which defines a zero-field magnetization $\mathbf{M}$ through $F_Z' = -\mathbf{M}\cdot\mathbf{H}$.

The dipole energy coefficient g_D cannot reliably be calculated from normal-state properties, but it can be determined from the measured longitudinal NMR frequency ν_L near the transition temperature:

$$g_D = \frac{1}{5}\frac{3\beta_{12}+\beta_{345}}{1+F_0^a}\frac{(h\nu_L)^2}{1-T/T_c} \ , \tag{8}$$

where repeated indices of β denote the sum of the corresponding β_i's. The weak-coupling expression for g_Z is

$$g_Z = \frac{7\zeta(3)}{48\pi^2}N(0)\left[\frac{\gamma_0\hbar}{(1+F_0^a)k_B T_c}\right]^2 \ . \tag{9}$$

Finally, g_Z', which is proportional to the particle-hole asymmetry, can be determined from the splitting of the A_1 transition $[A_{\mu j} \sim (\hat{\mathbf{x}} - i\hat{\mathbf{y}})_\mu(\hat{\mathbf{x}} + i\hat{\mathbf{y}})_j$, for example] at high magnetic fields:

$$g_Z' = \tfrac{1}{3}N(0)\frac{T_{A1}-T_c}{T_c H} \ . \tag{10}$$

All the effects considered in this paper follow from energy terms (1), (2), and (5)-(7). In addition to $\underline{\chi}$ and $\mathbf{M}$ defined above, some interesting observables are the supercurrent density

$$j_i = \frac{4m_3K}{\hbar}\operatorname{Im}[(\gamma-2)A_{\mu i}^*\partial_j A_{\mu j} + A_{\mu j}^*\partial_i A_{\mu j} + A_{\mu j}^*\partial_j A_{\mu i}] \tag{11}$$

and the spin-current density

TABLE I. Numerical values for the parameters of the GL theory at three different pressures. The parameters are calculated using formulas (3), (4), and (8)-(10) and the basic parameters $N(0)$, T_c, and v_F from Ref. 25, F_0^a from Ref. 26, β_3/β_3^{WC} from Ref. 27, ν_L from Refs. 28 and 29, and $T_{A1}-T_c$ from Refs. 30 and 31.

Pressure (bars)	$\alpha/(1-T/T_c)$ (10^{37} ergs^{-1} cm^{-3})	β_3 (10^{72} ergs^{-3} cm^{-3})	K (10^{25} ergs^{-1} cm^{-1})	g_D (10^{31} ergs^{-1} cm^{-3})	g_Z (10^{29} G^{-2}ergs^{-1} cm^{-3})	g_Z' (10^{31} G^{-1}ergs^{-1} cm^{-3})
34.36	3.95	6.68	4.04	5.63	1.19	6.37
18	2.96	6.51	6.18	3.30	1.15	3.59
0	1.67	21.6	41.9	3.25	2.33	1.27

$$j_{\kappa i}^{\mathrm{spin}} = -\frac{2}{\hbar}\epsilon_{\kappa\mu\nu}K\,\mathrm{Re}[(\gamma-2)A_{\mu i}^{*}\partial_j A_{\nu j}$$

$$+ A_{\mu j}^{*}\partial_i A_{\nu j} + A_{\mu j}^{*}\partial_j A_{\nu i}]\;. \tag{12}$$

Let us briefly consider the GL theory of the bulk B phase. Neglect first the small-energy terms (5)–(7). The maximum condensation energy density

$$f_c^B = 3\alpha^2/(12\beta_{12}+4\beta_{345}) \tag{13}$$

is achieved if the order parameter has the form

$$\underline{A} = \Delta\underline{R}(\hat{\mathbf{n}},\theta)e^{i\vartheta}\;. \tag{14}$$

Here $\Delta = [\alpha/(6\beta_{12}+2\beta_{345})]^{1/2}$ is the bulk gap. ϑ is an arbitrary phase angle, and $\underline{R}$ is an arbitrary rotation matrix, which describes the relative rotation of the spin and the orbit spaces. $\underline{R}$ is commonly parametrized by an axis of rotation $\hat{\mathbf{n}}$ and a rotation angle θ. The dipole energy (5) removes part of this degeneracy by fixing the angle at $\theta_0 = \arccos(-\frac{1}{4}) \approx 104°$ but leaves $\hat{\mathbf{n}}$ arbitrary. Finally, the magnetic energy (6) combined with (5) gives an orientation energy for $\hat{\mathbf{n}}$ as well:

$$F = -g_{DZ}\int d^3r(\hat{\mathbf{n}}\cdot\mathbf{H})^2\;, \tag{15}$$

where

$$g_{DZ} = \frac{5}{4}\frac{g_D g_Z}{\beta_{345}}\;. \tag{16}$$

The linear magnetic term (7) vanishes in the bulk.

For future reference it is useful to list the order parameters and energies of two other bulk phases as well. The bulk A-phase has the order parameter

$$\underline{A} = \Delta_A\hat{\mathbf{d}}(\hat{\mathbf{u}}_1+i\hat{\mathbf{u}}_2)\;, \tag{17}$$

where $\Delta_A^2 = \alpha/4\beta_{245}$ and $\hat{\mathbf{d}}$, $\hat{\mathbf{u}}_1$, and $\hat{\mathbf{u}}_2$ are arbitrary unit vectors except $\hat{\mathbf{u}}_1\cdot\hat{\mathbf{u}}_2 = 0$. The vectors $\mathbf{d}$ and $\hat{l}$ are defined by $\mathbf{d} = \Delta_A\hat{\mathbf{d}}$ and $\hat{l} = \hat{\mathbf{u}}_1\times\hat{\mathbf{u}}_2$, and the condensation energy is

$$f_c^A = \alpha^2/4\beta_{245}\;. \tag{18}$$

The planar phase is never stable in the bulk but it would have the order parameter

$$\underline{A} = \Delta_p\underline{R}(\hat{\mathbf{n}},\theta)(\underline{1}-\hat{\mathbf{w}}\,\hat{\mathbf{w}})\;, \tag{19}$$

where $\Delta_p^2 = \alpha/(4\beta_{12}+2\beta_{345})$ and $\hat{\mathbf{n}}$, θ, and $\hat{\mathbf{w}}$ are arbitrary. Its energy is

$$f_c^p = \alpha^2/(4\beta_{12}+2\beta_{345})\;. \tag{20}$$

III. FORMULATION OF THE VORTEX PROBLEM

The vortex is defined as a line defect of the superfluid around which the phase ϑ of the bulk B-phase order parameter (14) changes by 2π. This implies that far from the vortex line there is a circulating superfluid velocity

$$\mathbf{v}_s = \frac{\hbar}{2m_3}\nabla\vartheta = \frac{\hbar}{2m_3}\frac{\hat{\phi}}{r}\;. \tag{21}$$

Here r, ϕ, and z are the cylindrical coordinates and the vortex is along the z axis. The latter equality holds because an isolated vortex always has cylindrical symmetry at large r if the small-energy terms (5)–(7) are neglected. [This can be seen by substituting (14) into (1) and (2) and minimizing the energy with respect to $\vartheta(\mathbf{r})$]. It follows from Eq. (11) that there is an associated supercurrent density $\mathbf{j}_s = \rho_s\mathbf{v}_s$, where the superfluid density is given by

$$\rho_s = 2(\gamma+2)\left[\frac{2m_3}{\hbar}\right]^2 K\Delta^2\;. \tag{22}$$

The superfluid velocity (21) diverges at the vortex axis which implies that the bulk form of the order parameter (14) cannot be valid there. The determination of the vortex core is the main purpose of this paper.

Throughout this paper I assume the normal-fluid component to be at rest. Only in the comparison with experiments will the effect of the solid-body rotation of the normal fluid be taken into account.

The gradient energy (2) opposes rapid spatial variations of the order parameter. The characteristic length is different for different degrees of freedom in $\underline{A}$ depending how large is the driving energy for the spatial variations. For driving energies on the order of the whole superfluid condensation energy (1), the characteristic length is the GL (temperature-dependent) coherence length

$$\xi(T) = (K/\alpha)^{1/2} = \xi(0)/(1-T/T_c)^{1/2}\;. $$

This is the shortest length in the theory and it determines the size of the vortex core, $\xi(0) \approx 14$ nm. (All the numerical values are easily obtained from Table I and are in this paragraph given at 18 bars pressure.) For the dipole energy (5) the characteristic length is $\xi_D = (K/g_D)^{1/2} \approx 14$ μm. If the rotation angle deviates from 104°, it reverts to this value in a length $\approx \xi_D$. Often there is no force present to drive this deviation, so that $\theta = \theta_0$ everywhere. Finally, the combined field and dipole energy (15) gives a third length

$$\xi_{DZ} = (K\Delta^2/g_{DZ}H^2)^{1/2} \approx (8\ \mathrm{cm})\mathrm{G}(1-T/T_c)^{1/2}/H\;, $$

which is the healing length for the $\hat{\mathbf{n}}$ texture. [The quantity $(\frac{65}{8})^{1/2}H\xi_{DZ}$ is often called $R_C H_B$.] For all reasonable fields, ξ_{DZ} and ξ_D are much longer than $\xi(T)$ (except a very thin region near T_c which is not considered here). It follows that θ and $\hat{\mathbf{n}}$ are essentially constants across the vortex. This suggests for the order parameter the representation

$$\underline{A}(\mathbf{r}) = \Delta\underline{R}(\hat{\mathbf{n}},\theta)\underline{\tilde{A}}(\mathbf{r})\;, \tag{23}$$

where Δ and $\underline{R}$ are constants (independent of $\mathbf{r}$). To study the core structure of the vortex it is enough to solve for the reduced order parameter $\underline{\tilde{A}}$ and to take into account the energy terms (1) and (2) only. The matrix $\underline{R}$ in (23) is chosen such that the asymptotic form of the reduced order parameter is diagonal:

$$\lim_{r\to\infty}\underline{\tilde{A}}(r,\phi,z) = \underline{1}e^{i\phi}\;, \tag{24}$$

where $\underline{1}$ is the unit matrix. Once the solution for $\underline{\tilde{A}}$ is obtained, the true order parameter $\underline{A}$ is given by (23). Afterwards, one pays attention to the small-energy terms (5)–(7) calculating their contributions as a function of $\hat{n}$ (and θ).

Equation (24) above can be considered as a definition of a quantized vortex in ³He-*B*. One note should be made: sometimes an additional integer number m appears in the exponent, thus defining a multiple quantum vortex. Their flow energy outside the core is m^2 times that of a single-quantum vortex. Therefore it is extremely improbable that they occur in nature, even more so because they are

likely not even locally stable. If at very high rotation speeds ($\Omega > 10^5$ rad/s) the vortex lattice changes qualitatively, it is more probable that there is a transition to "spin-current vortices."[35,6]

The problem to be solved is the following: minimize the energies (1) and (2) requiring the boundary condition (24). One could apply numerical methods directly to this problem. This paper takes the alternative approach of first constructing a differential equation. This is achieved by the standard method of making a variation to the order parameter and requiring stationarity of the functional. The resulting GL differential equations can be written as

$$\tilde{\partial}_j \tilde{\partial}_j \tilde{A}_{\mu i} + (\gamma - 1)\tilde{\partial}_i \tilde{\partial}_j \tilde{A}_{\mu j} - [-\underline{\tilde{A}} + \tilde{\beta}_1 \underline{\tilde{A}}^* \mathrm{Tr}(\underline{\tilde{A}}\,\underline{\tilde{A}}^T) + \tilde{\beta}_2 \underline{\tilde{A}}\, \mathrm{Tr}(\underline{\tilde{A}}\,\underline{\tilde{A}}^{T*})$$
$$+ \tilde{\beta}_3 \underline{\tilde{A}}\,\underline{\tilde{A}}^T\underline{\tilde{A}}^* + \tilde{\beta}_4 \underline{\tilde{A}}\,\underline{\tilde{A}}^{T*}\underline{\tilde{A}} + \tilde{\beta}_5 \underline{\tilde{A}}^*\underline{\tilde{A}}^T\underline{\tilde{A}}]_{\mu i} = 0 \ . \tag{25}$$

This is a nonlinear elliptic partial-differential equation in three variables for the complex 3×3 matrix $\underline{\tilde{A}}$. Equation (25) has to be solved together with the boundary condition (24). In (25) the β coefficients and the partial derivatives appear in reduced units: $\tilde{\beta}_i = \beta_i / (3\beta_{12} + \beta_{345})$ and $\tilde{\partial}_i = \xi(T)\partial_i$.

It is useful to consider the symmetries of the problem, i.e., to list the symmetry operations that leave the problem unchanged. The continuous symmetries are (a) the translational symmetry in the z direction and (b) the rotational symmetry around z combined with phase multiplication by the same angle. The latter is denoted by $\exp(i\vartheta)C^z_\vartheta$, where ϑ is the rotation angle. The problem has two basic reflection symmetries, which are (c) reflection in the x-y plane (σ^z) and (d) reflection in the x-z plane combined with time inversion and a phase change by $\pi(-T\sigma^y)$. The time inversion simply reduces to complex conjugation in the present case. Finally, (e) all the other symmetry operations can be constructed as combinations of (a)–(d).

One can give more precise definitions of the symmetry operations. For example, the symmetry operation (b) transforms the order parameter field $\underline{\tilde{A}}$ into a field that is denoted by $\exp(i\vartheta)C^z_\vartheta\underline{\tilde{A}}$, the value of which at position $\mathbf{r}$ is equal to

$$e^{i\vartheta}\underline{R}(\hat{z},\vartheta)\underline{\tilde{A}}[\underline{R}^{-1}(\hat{z},\vartheta)\mathbf{r}]\underline{R}^{-1}(\hat{z},\vartheta) \ . \tag{26}$$

Note that the rotation has to be combined with a phase change in this combination; neither alone is a symmetry of the problem because they violate the boundary condi-

tion (24). Another example:

$$(-T\sigma^y\underline{\tilde{A}})(\mathbf{r}) = -\underline{S}_y\underline{\tilde{A}}^*(\underline{S}_y^{-1}\mathbf{r})\underline{S}_y^{-1} \ , \tag{27}$$

where $\underline{S}_y$ is a diagonal matrix with elements 1, -1, and 1.

In general, either all the symmetries of a problem are satisfied by the solution or, alternatively, one or more symmetries are broken in the solution. Also, one can often simplify the original problem by exploiting the symmetries which are known not to be broken. In the present problem [(24) and (25)], however, one must be very careful in assuming any symmetries because only one solution with maximum symmetry has been found[7] and it is not enough to explain the observed transition. The problem would be essentially simpler if the axial translational symmetry (a) or the axial rotational symmetry (b) of the solution could be guaranteed. There is a decisive difference between these two: the former is a pure translational symmetry but the latter is combined with a phase winding, i.e., there is a supercurrent in the direction of the symmetry. There are many cases where the translational symmetry in the direction of the current is broken—the mere existence of vortices is a demonstration of this—but there is no known case of breaking the pure translational symmetry in any superfluid problem. Therefore, in the following analysis the solution is assumed to be constant in the z direction, but no further assumptions are made. This assumption is further discussed at the end of Sec. V.

The translational symmetry of the solution in the z direction simplifies the GL equation into the form

$$(\gamma\tilde{\partial}_x^2 + \tilde{\partial}_y^2)\tilde{A}_{\mu x} + (\gamma - 1)\tilde{\partial}_x\tilde{\partial}_y\tilde{A}_{\mu y} - [-\underline{\tilde{A}} + \tilde{\beta}_1\underline{\tilde{A}}^*\mathrm{Tr}(\underline{\tilde{A}}\,\underline{\tilde{A}}^T) + \tilde{\beta}_2\underline{\tilde{A}}\,\mathrm{Tr}(\underline{\tilde{A}}\,\underline{\tilde{A}}^{T*})$$
$$+ \tilde{\beta}_3\underline{\tilde{A}}\,\underline{\tilde{A}}^T\underline{\tilde{A}}^* + \tilde{\beta}_4\underline{\tilde{A}}\,\underline{\tilde{A}}^{T*}\underline{\tilde{A}} + \tilde{\beta}_5\underline{\tilde{A}}^*\underline{\tilde{A}}^T\underline{\tilde{A}}]_{\mu x} = 0 \ ,$$

$$(\tilde{\partial}_x^2 + \gamma\tilde{\partial}_y^2)\tilde{A}_{\mu y} + (\gamma - 1)\tilde{\partial}_x\tilde{\partial}_y\tilde{A}_{\mu x} - [-\underline{\tilde{A}} + \tilde{\beta}_1\underline{\tilde{A}}^*\mathrm{Tr}(\underline{\tilde{A}}\,\underline{\tilde{A}}^T) + \tilde{\beta}_2\underline{\tilde{A}}\,\mathrm{Tr}(\underline{\tilde{A}}\,\underline{\tilde{A}}^{T*}) \tag{28a}$$
$$+ \tilde{\beta}_3\underline{\tilde{A}}\,\underline{\tilde{A}}^T\underline{\tilde{A}}^* + \tilde{\beta}_4\underline{\tilde{A}}\,\underline{\tilde{A}}^{T*}\underline{\tilde{A}} + \tilde{\beta}_5\underline{\tilde{A}}^*\underline{\tilde{A}}^T\underline{\tilde{A}}]_{\mu y} = 0 \ ,$$

$$(\tilde{\partial}_x^2 + \tilde{\partial}_y^2)\tilde{A}_{\mu z} - [-\underline{\tilde{A}} + \tilde{\beta}_1\underline{\tilde{A}}^*\mathrm{Tr}(\underline{\tilde{A}}\,\underline{\tilde{A}}^T) + \tilde{\beta}_2\underline{\tilde{A}}\,\mathrm{Tr}(\underline{\tilde{A}}\,\underline{\tilde{A}}^{T*}) + \tilde{\beta}_3\underline{\tilde{A}}\,\underline{\tilde{A}}^T\underline{\tilde{A}}^* + \tilde{\beta}_4\underline{\tilde{A}}\,\underline{\tilde{A}}^{T*}\underline{\tilde{A}} + \tilde{\beta}_5\underline{\tilde{A}}^*\underline{\tilde{A}}^T\underline{\tilde{A}}]_{\mu z} = 0 \ .$$

This is now a partial-differential equation in two variables x and y. The boundary condition for the 3×3 complex matrix $\underline{\tilde{A}}$ now reads

$$\lim_{r \to \infty} \underline{\tilde{A}}(r,\phi) = \underline{1} e^{i\phi} . \tag{28b}$$

The symmetries of the problem are (b)–(e) mentioned above, as the symmetry (a) is taken unbreakable.

IV. THE VORTEX SOLUTIONS

In the preceding section the physical problem of studying vortices was put in a concise mathematical form (28). In this section three solutions of Eq. (28) are described. Based on the symmetries of the problem, one can divide all the possible solutions into classes according to their symmetries in the same way as one can classify all the Bravais lattices, for example.[10] The vortex problem (28) is relatively simple because it only has point symmetries and the possible symmetry groups of the solutions can be read directly from Ref. 36. They are C_n, S_{2n}, C_{nh}, C_{nv}, D_n, D_{nh}, and D_{nd} ($n = 1, 2, \ldots, \infty$; S_{2n} and D_{nd} are not defined at $n = \infty$). The classification of Ref. 9 is a special case of this having $n = \infty$.

There are only two physical (local minima of the free energy) vortex solutions: the A-phase-core vortex and the double-core vortex. However, it is instructive to study first the normal-core vortex. This vortex has the maximum symmetry (symmetry group $D_{\infty h}$) and it is the vortex that mostly resembles the vortices in ^{4}He and in superconductors. As shown in Fig. 2(a) all the elements of the order-parameter vanish at the vortex center as required by the symmetries. For example, the rotational symmetry of the solution implies that the order-parameter field $\exp(i\vartheta)C_\vartheta^z\underline{\tilde{A}}$ given by (26) is identical to $\underline{\tilde{A}}$ for all ϑ. In the vortex center this constraint reduces $\underline{\tilde{A}}$ to the form

$$\underline{\tilde{A}}(0,0) = \begin{bmatrix} 0 & 0 & a_2 \\ 0 & 0 & ia_2 \\ a_1 & ia_1 & 0 \end{bmatrix} , \tag{29}$$

where a_1 and a_2 are complex numbers. The symmetry $-T\sigma^y$ [Eq. (27)] reduces a_1 and a_2 to be real. Finally, the symmetry σ^z requires a_1 and a_2 to vanish. On the x axis the symmetries constrain the order parameter of the normal-core vortex to the form

$$\underline{\tilde{A}}(x,0) = \begin{bmatrix} b_1 & ib_2 & 0 \\ ib_3 & b_4 & 0 \\ 0 & 0 & b_5 \end{bmatrix} , \tag{30}$$

where the b_i's are real functions of x [displayed in Fig. 2(a)]. This defines the order parameter everywhere because of the rotational symmetry. Far from the core, $\underline{\tilde{A}}$ is determined by the flow field (21) and it can be calculated
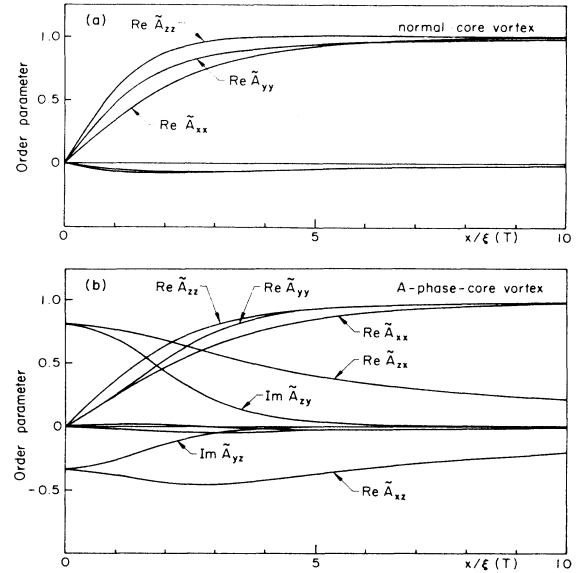
FIG. 2. The order parameter of (a) the normal-core vortex and (b) the A-phase-core vortex in the weak coupling. $\underline{\tilde{A}}$ is shown in rectangular coordinates on the x axis. This defines $\underline{\tilde{A}}$ everywhere because of the rotational symmetry $[\exp(i\vartheta)C_\vartheta^z]$. The imaginary parts of $\tilde{A}_{xy}$ and $\tilde{A}_{yx}$ are small but nonzero. Noteworthy features in (b) are the slow decay of $\mathrm{Re}\,\tilde{A}_{xz}$ and $\mathrm{Re}\,\tilde{A}_{zx}$ towards the bulk and the A-phase core by $\mathrm{Re}\,\tilde{A}_{zx}$ and $\mathrm{Im}\,\tilde{A}_{zy}$. The rotational symmetry requires $\tilde{A}_{zy} = i\tilde{A}_{zx}$ and $\tilde{A}_{yz} = i\tilde{A}_{xz}$ at the vortex center.

analytically:[7]

$$\underline{\tilde{A}}^{(0)}(x,0) = \begin{bmatrix} 1+c_1 & ic_3 & 0 \\ ic_3 & 1+c_2 & 0 \\ 0 & 0 & 1+c_1 \end{bmatrix} + O(x^{-3}) ,$$

$$c_1 = [(\gamma+2)\tilde{\beta}_{12} - 1]/(2\tilde{\beta}_{345})[\xi(T)/x]^2 ,$$

$$c_2 = [(\gamma+2)\tilde{\beta}_{12} - \gamma]/(2\tilde{\beta}_{345})[\xi(T)/x]^2 , \tag{31a}$$

$$c_3 = (\gamma-1)/(6\tilde{\beta}_1)[\xi(T)/x]^2 .$$

Note that the deviations from the unit matrix decay as r^{-2} and their amplitude is fixed by the circulating flow.

The A-phase-core vortex breaks the σ^z symmetry, leaving the symmetry group $C_{\infty v}$. This allows an order parameter of the form (29) with a_1 and a_2 finite and real in the vortex core. The parameter a_1 is the amplitude of the A phase (17) in the vortex core and calculations show that it is always larger than a_2. The A phase in the center always has the $\hat{l}$ vector in the direction of $+\hat{z}$ and the $\mathbf{d}$ vector in the direction $\pm\underline{R}(\hat{n},\theta)\hat{z}$. Broken σ^z symmetry implies broken parity: the A-phase-core vortex is either right-handed or left-handed depending on the direction of $\mathbf{d}$. The complete order parameter is shown in Fig. 2(b).

An important feature of the A-phase-core vortex is that it does not obey the asymptotic form (31a): the real components $\tilde{A}_{xz}$ and $\tilde{A}_{zx}$ decay slowly, as r^{-1}. This can be understood as follows:[12] the superfluid condensation en-

ergy of the B phase is independent of the rotation of the spin space with respect to the orbital space. Therefore, a position-dependent spin rotation costs only gradient energy and it can heal slowly. The asymptotic structure of the A-phase-core vortex has, in addition to (31a), terms describing a spin rotation around the azimuthal direction $\hat{\phi}$:

$$\tilde{\underline{A}}(x,0)=\tilde{\underline{A}}^{(0)}(x,0)+c_4\begin{bmatrix}0 & 0 & -1\\0 & 0 & 0\\1 & 0 & 0\end{bmatrix}\frac{\xi(T)}{x}$$

$$+c_4\begin{bmatrix}-\frac{1}{2} & 0 & 0\\0 & 0 & 0\\0 & 0 & -\frac{1}{2}\end{bmatrix}\left[\frac{\xi(T)}{x}\right]^2. \qquad (31b)$$

The analysis of the asymptotic leaves the real rotation amplitude c_4 arbitrary and it can be determined only by solving $\tilde{\underline{A}}$ for the whole vortex.

In the double-core vortex the continuous rotational symmetry around the vortex axis is broken. The only symmetries left are (choosing the coordinate axes appropriately) the reflection symmetry in the x-z plane $(-T\sigma^y)$, the reflection in the y-z plane $(T\sigma^x)$, and their

product, which is a discrete rotational symmetry around the vortex axis by $180°$ $(-C_\pi^z)$ (symmetry group C_{2v}). Requiring only the discrete rotational symmetry relaxes the form (29) to

$$\tilde{\underline{A}}(0,0)=\begin{bmatrix}0 & 0 & a_2\\0 & 0 & ia_4\\a_1 & ia_3 & 0\end{bmatrix} \qquad (32)$$

in the center of the vortex. The reflection symmetries constrain the a_i's to be real numbers. The dominant of these are $a_1\approx-a_2\approx1$, which form a planar phase (19). This planar phase has a $90°$ spin rotation around y, and the vector $\hat{\mathbf{w}}$ is in the y direction. The presentation of the complete order parameter is complicated because of the lack of the cylindrical symmetry. Figure 3 displays the order parameter on the symmetry axes x and y. There are nine nonzero components in these directions but in other directions all the 18 real degrees of freedom are nonzero. Reference 37 displays one of the components in the x-y plane. The asymptotic form of the order parameter is similar to the A-phase-core vortex on the symmetry axes but the rotation amplitudes are different in different directions [Eq. (31b) is valid on the x axis and is slightly modified on the y axis], the rotation on the x axis around y being much larger than on the y axis around x.

In the double-core vortex on the x axis the Cooper pairs having momenta in the x and z direction experience only a slow spin rotation by $180°$ as x goes from $-\infty$ to $+\infty$. This is illustrated in Fig. 4. The Cooper pairs having momenta in the y direction are like those in the normal-core vortex, i.e., their pairing amplitude (approximately) vanishes at the center of the vortex. On the y axis things are quite different: the bulk B phase $(\tilde{\underline{A}}\approx\pm i\underline{1})$ is out of phase from the planar phase in the center and there is a clear interface between them at $y\approx\pm3\xi(T)$. It is instructive to study the quantity

$$\tfrac{1}{3}\mathrm{Tr}(\tilde{\underline{A}}\,\tilde{\underline{A}}^{T*})\,, \qquad (33)$$

which could loosely be called the superfluid density. It is displayed in Fig. 5. It has minima at the two points on
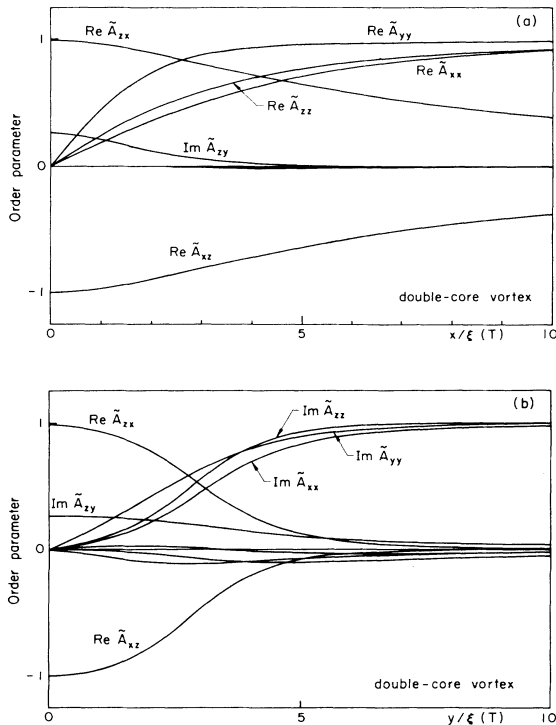
FIG. 3. The order parameter of the double-core vortex (a) on the x axis and (b) on the y axis in weak coupling. In (a) the imaginary parts of A_{xy}, A_{yx}, and A_{yz} are small but nonzero. In (b) the real parts of A_{xy} and A_{yx} and the imaginary part of A_{yz} are small but nonzero. In intermediate directions all the 18 degrees of freedom are nonzero. On the x axis the order parameter has a smooth spin rotation but on the y axis there is an abrupt change from the center to the bulk B phase at $y\approx\pm3\xi(T)$.
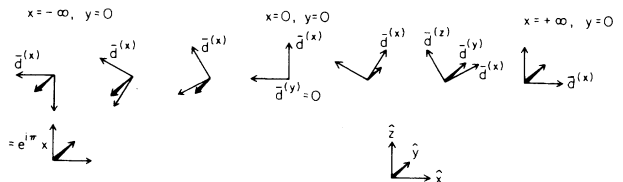
FIG. 4. The qualitative behavior of the order parameter (vectors $\mathbf{d}^{(x)}=\tilde{\underline{A}}\hat{\mathbf{x}}$, $\mathbf{d}^{(y)}=\tilde{\underline{A}}\hat{\mathbf{y}}$, and $\mathbf{d}^{(z)}=\tilde{\underline{A}}\hat{\mathbf{z}}$) on a path from $(x,y)=(+\infty,0)$ to $(-\infty,0)$ that passes between the cores in the double-core vortex. On a path passing both cores on the same side, these vectors preserve their directions but have a phase factor $\exp(i\phi)$, where ϕ is the azimuthal angle. All the paths end up with the same order parameter at $x=-\infty$; that is, $\exp(i\pi)$ times the order parameter at $x=+\infty$, in accordance with (28b).
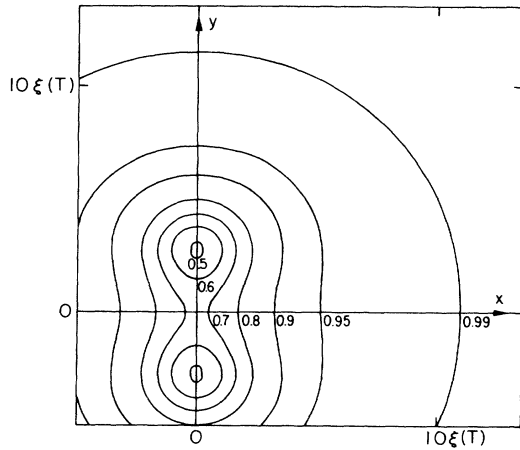
FIG. 5. The "superfluid density" (33) for the double-core vortex in weak coupling. The corresponding plot for the A-phase-core vortex is a series of concentric circles and it is evaluated in Ref. 38.

the y axis, which can be called the cores of the vortex. The trapping potential of ions is proportional to this quantity.[39]

The double-core character is also displayed in Fig. 6, which shows the supercurrent (11) around the vortex. Unlike the others, the double-core vortex has a nonvanishing *axial* supercurrent (although there is no phase gradient in the z direction). By symmetry, the current has opposite directions in different quadrants of the plane (Fig. 7) and the integrated current is zero. (Were it not, it would imply an instability towards creating a phase gradient in the z direction.) The vortex core also has a complicated pattern of spin currents (12).

V. ENERGIES

It is practical to express the energies (and other physical quantities of the vortices) relative to the bulk B phase and per unit length. Far from the vortex axis the superflow (21) gives an energy density $\rho_s v_s^2/2$. Because it diverges logarithmically when integrated over the vortex, we
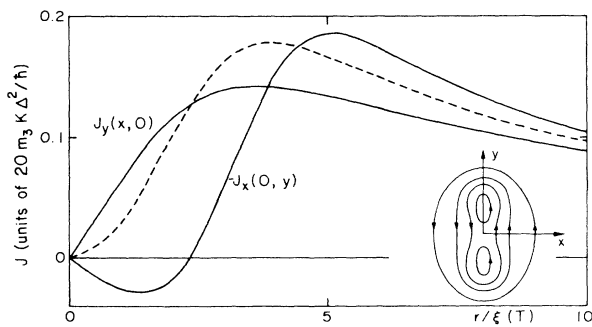
FIG. 6. The supercurrent around the vortex on the x and the y axes in units 20 $m_3 K\Delta^2/\hbar$ (weak coupling). The inset sketches some flow lines which display the double-core nature of the vortex. In the A-phase-core vortex the flow has cylindrical symmetry and it is shown by the dashed line in the figure.
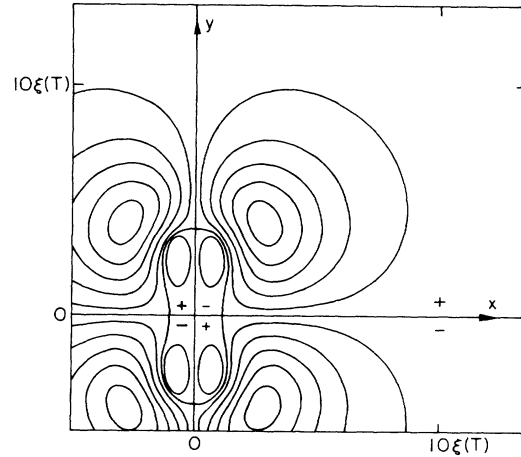
FIG. 7. The axial supercurrent in the double-core vortex (weak coupling). The current vanishes on the x and the y axes, its maximum value is 0.006 in units $20m_3 K\Delta^2/\hbar$, and its direction ($\pm z$) is denoted by signs. The axial supercurrent is zero in the A-phase-core vortex.

separate it from all the other contributions to the energy and write

$$F = f_c^B \xi^2(T)\left[\tilde{F} + \frac{4\pi(\gamma+2)}{3}\ln\left[\frac{R}{\xi(T)}\right]\right] . \quad (34)$$

Here f_c^B is the condensation energy density of the bulk B phase (13). The second term in (34) can be called the asymptotic energy and it is cut off at some large radius $R \gg \xi(T)$. This term is the same for all vortices. The energy differences between vortices are contained in $\tilde{F}$ and it is shown in Fig. 8 as a function of pressure.
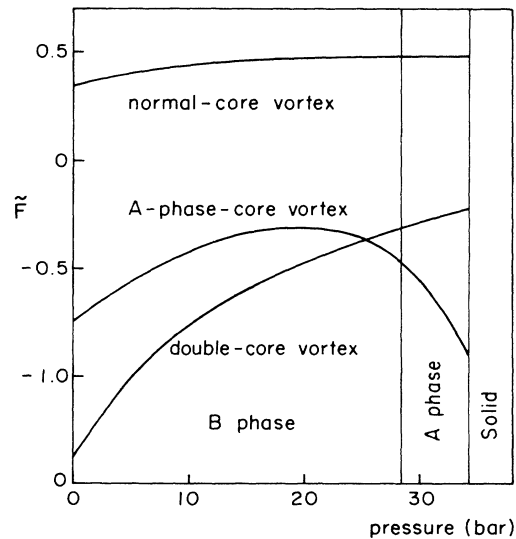
FIG. 8. The vortex energies $\tilde{F}$, Eq. (34), as a function of pressure. The energy is expressed in units of $f_c^B \xi^2(T)$, which has simple interpretation as the area in square $\xi(T)$'s of the bulk condensation energy.

The energy of the normal-core vortex is higher than of the other two at all pressures. The double-core vortex is the absolute energy minimum at low pressures and the A-phase-core vortex at high pressures. These latter two remain locally stable in the superheated B phase up to the melting pressure. The normal-core vortex is not locally stable at any pressures but is a saddle point of energy.[9,11] According to my numerical studies, the A-phase-core vortex is also unstable in the weak-coupling limit and becomes locally stable only at elevated pressures; I was unable to get convergence to the A-phase-core vortex unless I constrained the solution to have the rotational symmetry. This is contrary to the result of Salomaa and Volovik[17] and the reason for this is not known. Presumably it cannot be due to their basic ansatz because it should be exact in studying the local stability of the A-phase-core vortex.

One can qualitatively understand the energies as follows, see Fig. 9. The normal-core vortex has the highest energy because it does not have superfluid condensation in the core. The existence of the core superfluidity is favored if more condensation energy is gained in the vortex center than lost in the increased gradient energy in the interface between the center phase and the B phase. The double-core vortex has especially low energy at low pressures because the planar phase transforms smoothly to the bulk B phase near the x axis and interface energy is lost only near the y axis. The A-phase-core vortex loses interface energy in all directions but it becomes favored at high pressures because the A phase has lower energy there than the planar phase.

The increased condensation energy of the A relative to the B phase extends the core of the A-phase-core vortex at high pressures but the increasing interface area (and energy) keeps it bounded. Considering the energies of the two bulk phases and their interface, it is simple to see that the A-phase-core vortex remains stable in the superheated B phase for some finite range of pressures and numerical calculations show that this range extends over the whole A phase region. Thus the vortices do not act as a nucleation center for the A phase if thermal fluctuations are neglected, contrary to Ref. 9.
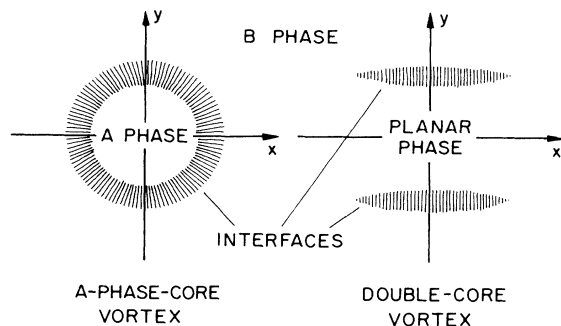
FIG. 9. The bulk and center phases and their interfaces in the physical vortices. The cores of the double-core vortex are bounded together by the planar phase because it has lower condensation energy than the bulk B phase.

The energy of an interface between two phases in general depends on the orientations of the phases.[40] In both physical vortices, the slowly decaying spin rotation of the B phase outside the core (31b) is a consequence of the B phase trying to orient itself in order to minimize the interface energy. This also qualitatively explains the absence of the vortices having symmetries σ^z or $-T\sigma^y\sigma^z$ (u or w vortices and their nonaxisymmetric generalizations according to Ref. 9). These vortices also could have an A or a planar phase in the center but they do not allow the minimal interface energy.

The energy diagram (Fig. 8) identifies the vortex observed at the high-pressure–high-temperature corner of the phase diagram (Fig. 1) as the A-phase-core vortex and the vortex observed elsewhere as the double-core vortex. The theory gives the transition at approximately 3 bars below the tricritical pressure. It is noteworthy that the theory has no adjustable parameters and only normal-state data in addition to $T_c(p)$ are needed in the calculation. The transition is first order because both vortices preserve their identity on both sides of the transition. The symmetries alone could have allowed a second-order transition between the vortices because all the symmetries of the double-core vortex are present in the A-phase-core vortex as well. Thus it was an incorrect suggestion that one could rule out some vortex candidates on the basis of their symmetries.[8]

It is noteworthy that the simple weak-coupling β coefficients produce the more complicated, double-core vortex and the simpler A-phase-core vortex can be obtained only if strong-coupling corrections to β_i's are taken into account. It would require some numerical effort to map the stability regions of the different vortices in the general five-dimensional β_i space, but the simple qualitative argument above indicates that the A-phase-core vortex is most probably found in places where the condensation energy of the A phase (18) is highest relative to that of the planar phase (20).

The present numerical method solves the problem of Eq. (28) exactly by iteration. It is unlikely that there are other physical solutions than those described above: various initial guesses for the iteration were tried, including several having no symmetries at all, but no solutions breaking the symmetries of the double-core vortex were found. An indication that the search has been complete enough (at least in some subspace of solutions) is that the same fourth vortex solution was found independently by Salomaa and Thuneberg (unpublished). This solution (having discrete rotation symmetry by 90°: $iC_{\pi/2}^z\sigma^z$) is completely unphysical because it is a saddle point of the energy (which is slightly lower than that of the normal-core vortex) and the iteration converges to it only if special symmetry constraints are imposed on the solution. The only doubt on the present identification of the vortices is raised by the possible breaking of the translational symmetry along the vortex axis. Such a possibility was argued against in Sec. III, but let us consider it further: It is, in principle, possible to break the continuous symmetry into a discrete one; but, however, the continuous symmetry most likely remains but combined with another symmetry. The only such possibility is a helical deforma-

tion of the double-core vortex, which was suggested by Salomaa and Volovik[17] to explain the observed metastable state at low temperatures (see Sec. VIII). The double-core vortex could either have instability against small helicity or large helicity. The former possibility was recently studied numerically by Schopohl,[41] who found the double-core vortex stable. Also, the experimental metastability can be understood without invoking helical vortices as will be discussed in Secs. VII and VIII. Therefore, there is no evidence in favor of helical vortices.

VI. THE NUMERICAL METHOD

The problem (28) was solved numerically. The x and y variables were discretized with equal steps Δx to a square lattice (x_n, y_m). The derivatives were expressed by the simplest difference formulas[42] and in the computer program the order parameter was treated as a three-dimensional complex matrix exactly in the same form as in (28a). Starting from an initial guess $\underline{\tilde{A}}^{(0)}(x_n, y_m)$, the order parameter was iterated to convergence. There are two ways to derive the iteration formula used. The first approach is the Newton method in function space:[43]

$$\underline{\tilde{A}}^{(n+1)} = \underline{\tilde{A}}^{(n)} - [\underline{G}'(\underline{\tilde{A}}^{(n)})]^{-1} \underline{G}(\underline{\tilde{A}}^{(n)}) , \qquad (35)$$

where $\underline{G}(\underline{\tilde{A}})$ represents the (discretized) left-hand side of (28a), i.e., (28a) is equivalent to $\underline{G}(\underline{\tilde{A}}) = 0$, and $\underline{G}'$ is the derivative of $\underline{G}$. It is standard to neglect the off-diagonal part of $\underline{G}'$ in x-y space. In the present work, (35) was further simplified by assuming $\underline{G}' \approx -\underline{1}c^{-1}$, where c is some real parameter. Written more explicitly,

$$\underline{\tilde{A}}^{(n+1)}(x_n, y_m) = \underline{\tilde{A}}^{(n)}(x_n, y_m) + c\underline{G}(x_n, y_m; \underline{\tilde{A}}^{(n)}) . \qquad (36)$$

The parameter c was chosen "experimentally" to get the fastest convergence. A second way to understand (36) is to note that it is the time discretization of what is commonly known as the time-dependent GL equation:

$$\frac{\partial \underline{\tilde{A}}(x_n, y_m)}{\partial t} = -a \frac{\delta F(\underline{\tilde{A}})}{\delta \underline{\tilde{A}}^{T*}(x_n, y_m)} . \qquad (37)$$

Here F is the free-energy functional (1) and (2) and the correspondence with (36) is obtained by noting

$$\underline{G} \sim -\frac{\delta F}{\delta \underline{\tilde{A}}^{T*}} \qquad (38)$$

and $c \sim t^{(n+1)} - t^{(n)}$. The free energy F was discretized in x and y so that Eq. (38) remains valid.[43] It is simple to prove that in (37) the energy is a nonincreasing quantity. This implies that (36) can only proceed towards lower energy if c is sufficiently small (and positive).

The boundary condition (28b) was implemented in three different ways: (a) fixing the value of $\underline{\tilde{A}}$ according to (31a), (b) fixing the normal derivative of $\underline{\tilde{A}}$ to zero, and (c) fixing the value of $\underline{\tilde{A}}$ as in (31a) but multipiled by an arbitrary rotation matrix. The last method allowed the smallest computational cutoff radius R_c $(x_n^2 + y_m^2 < R_c^2)$. The solution was independent of the boundary condition used if R_c was sufficiently large.

The advantage of (36) is that it is very simple to pro-

gram. The rectangular coordinates also produce no artificial singularities. The computing times depend on the parameters used (lattice spacing, cutoff radius, type of vortex, reflection symmetries exploited, and needed degree of convergence) and there is, of course, no upper limit to the time used. Surprisingly, all the qualitative and also most quantitative results of this paper can be obtained using lattice constant Δx as large as $\xi(T)$, and the fastest convergence is obtained with $c \approx 0.1$. For $R_c \approx 10\xi(T)$ the computing time is a couple of minutes on a fast computer. To increase the accuracy, one has to increase R_c and decrease Δx. Halving the lattice spacing (optimal $c \approx 0.02$) increased the computing time considerably. This mainly changed the absolute energy and only slightly affected the order parameter, the susceptibility, the magnetization (which changed by a few percent) and the relative energies of the vortices (which shifted the transition pressure by 2 bars).

VII. MAGNETIC PROPERTIES

The previous analysis was based exclusively on the energy terms (1) and (2). In this section we study the smaller-energy terms (5)–(7), which also provide the means of studying the vortices experimentally.

Let us consider the dipole energy (5) first. The true order parameter $\underline{A}$ can be obtained from the numerically computed $\underline{\tilde{A}}$ by multiplying by the spin-rotation matrix $\underline{R}$, Eq. (23). This makes the dipole energy a function of the rotation parameters θ and $\hat{n}$. The bulk liquid fixes the rotation angle at $\theta_0 = 104°$ and dilute vortices cannot change that much. In contrast, $\hat{n}$ is not oriented by the bulk in the absence of magnetic field and so it is determined by the vortices (and the boundaries of the container). We are interested only in the anisotropy of the dipole energy, not in the absolute value because it is vanishingly small compared to the bulk condensation energy.

One deduces from the asymptotic form (31) that the dipole-energy anisotropy is logarithmically divergent and has to be represented in the form

$$F_D(\hat{n}) = g_D \Delta^2 \xi^2(T) \left[a_D(\hat{n}) + b_D(\hat{n}) \ln \frac{R}{\xi(T)} \right] , \qquad (39)$$

where the coefficients a_D and b_D depend on the vortex and the cutoff radius R appears in the second term only. For the normal-core vortex

$$b_D(\hat{n} = \hat{z}) - b_D(\hat{n} \perp \hat{z}) = \frac{5\pi(\gamma - 1)}{2\tilde{\beta}_{345}} . \qquad (40)$$

For the physical vortices the coefficients a_D and b_D are listed in Table II in the symmetry directions. One needs to display F_D in two octants of the full $\hat{n}$ sphere in order to represent it completely for the double-core vortex, but to a good approximation

$$F_D(\hat{n}) \approx F_D(\hat{x}) n_x^2 + F_D(\hat{y}) n_y^2 + F_D(\hat{z}) n_z^2 , \qquad (41)$$

because this is exact in the asymptotic region and the largest contribution comes from there.

The lowest dipole energy for the normal-core vortex is achieved with $\hat{n}$ in the x-y plane, for the A-phase-core

TABLE II. The dipole-energy coefficients of (39) for the physical vortices at zero pressure. The arbitrariness of the zero-point energy is used to put some coefficients to zero. The coefficient b_D is the dominant one for reasonable cutoffs. The numbers are approximate.

	A-phase-core vortex		Double-core vortex		
	$\hat{\mathbf{n}} \perp \hat{\mathbf{z}}$	$\hat{\mathbf{n}} = \hat{\mathbf{z}}$	$\hat{\mathbf{n}} = \hat{\mathbf{x}}$	$\hat{\mathbf{n}} = \hat{\mathbf{y}}$	$\hat{\mathbf{n}} = \hat{\mathbf{z}}$
a_D	-85	5	-4	-290	0
b_D	65	0	-20	320	0

vortex with $\hat{\mathbf{n}} = \hat{\mathbf{z}}$, and for the double-core vortex with $\hat{\mathbf{n}} = \hat{\mathbf{x}}$. This seemingly complicated behavior has a simple physical explanation in terms of the asymptotic form (31). If the order parameter $\underline{A}$ is almost diagonal as in (31a), the dipole energy (5) is minimized with $\hat{\mathbf{n}}$ pointing in the direction where the superfluidity is at the weakest. The azimuthal current preferentially depairs the order-parameter component parallel to the current which explains the minimum-energy direction $\hat{\mathbf{n}} \perp \hat{\mathbf{z}}$ in the normal-core vortex. The same mechanism is present in the physical vortices as well but it is dominated by another effect: If the long-range spin-rotation contained in $\underline{A}$, (31b), and the explicit rotation $\underline{R}(\hat{\mathbf{n}}, \theta_0)$ are around the same direction, the total rotation angle can greatly deviate from the optimum θ_0, giving increased dipole energy. This explains the large dipole energies of $\hat{\mathbf{n}} \perp \hat{\mathbf{z}}$ in the A-phase-core vortex and $\hat{\mathbf{n}} = \hat{\mathbf{y}}$ in the double-core vortex.

Out of the magnetic field terms, let us consider the susceptibility (6) first. In the bulk it gives a reduction $-2g_Z\Delta^2\underline{1}$ to the susceptibility of the normal Fermi liquid and it is convenient to express the susceptibilities relative to this bulk B-phase value: $\delta\underline{\chi} = \underline{\chi} - \chi^B$. The asymptotic form (31) gives a logarithmically divergent contribution and the susceptibility of the vortex has to be written as

$$\delta\underline{\chi} = \delta\underline{\chi}^{\text{core}} + (\underline{1} - \hat{\mathbf{z}}'\hat{\mathbf{z}}')g_Z\Delta^2\xi^2(T)\frac{2\pi(\gamma-1)}{\tilde{\beta}_{345}}\ln\left[\frac{R}{\xi(T)}\right].$$

(42)

Here $\hat{\mathbf{x}}' = \underline{R}\hat{\mathbf{x}}$, $\hat{\mathbf{y}}' = \underline{R}\hat{\mathbf{y}}$, and $\hat{\mathbf{z}}' = \underline{R}\hat{\mathbf{z}}$ are a convenient set of basis vectors in the spin space which make $\underline{\chi}$ diagonal. The latter term in (42) is independent of the type of the vortex. The susceptibilities are shown in Fig. 10 as a function of pressure.

It is simple to understand a couple of features in Fig. 10 physically. Most of the difference between the upper and the lower curves comes from the second term in (42) that is cut off at $R = 10^4\xi(T)$. The high-susceptibility anisotropy of the A-phase-core vertex is explained by the core A phase: the susceptibility is strongly reduced in the direction of $\mathbf{d}$ vector ($\mathbf{d} = \pm\hat{\mathbf{z}}'$) and increased in other directions. The susceptibility of the double-core vortex is greatest in the y' direction because the superfluidity is weakest in the corresponding orbital direction y.

The zero-field magnetic moment is defined by (7). The nonunitariness of the asymptotic form (31) gives rise to a magnetic moment density

$$\mathbf{m}(\mathbf{r}) = \frac{1}{6}g_Z'\Delta^2\hat{\mathbf{z}}'\frac{(\gamma-1)^2}{|\tilde{\beta}_1|\tilde{\beta}_{345}}\left[\frac{\xi(T)}{r}\right]^4 + O(r^{-5}).$$

(43)

The integrated magnetic moments are shown in Fig. 11 as a function of pressure. All the vortices have magnetic moments only in the $-\hat{\mathbf{z}}'$ direction. This is just opposite to the asymptotic form and thus the dominant magnetization comes from the vortex-core region. The physical vortices show magnetic moment densities in the other directions that are generally several times larger than in the $\hat{\mathbf{z}}'$ direction but they always cancel in the integrated moment.

Table II and Figs. 10 and 11 summarize the interaction of the vortices and the $\hat{\mathbf{n}}$ texture. The equilibrium texture in specific experimental configurations can be deduced from them using the texture theory.[19,44] The experiments of Hakonen et al. are discussed in the next section. This section will be concluded by applying these results to two more general questions: the orienta-
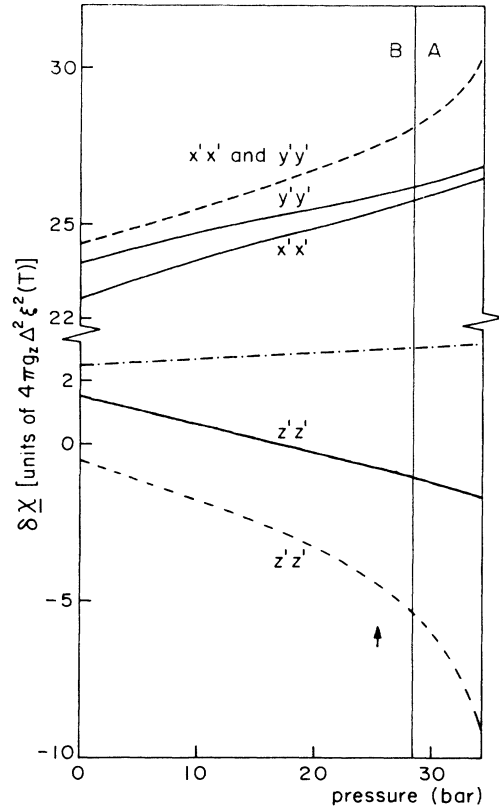
FIG. 10. The components of the susceptibility tensor for the double-core vortex (solid lines) and for the A-phase-core vortex (dashed lines) as a function of pressure. To simplify the comparison with Ref. 9, the full $\delta\underline{\chi}$ in (42) is displayed with $R = 10^4\xi(T)$ and in units of $4\pi g_Z\Delta^2\xi^2(T)$. The numbers have a simple interpretation being the (direction-dependent) effective area/2π [units of $\xi^2(T)$] in which the bulk B phase is replaced by the normal state in the vortex. To simplify the transformation to different R's, the prefactor $\tilde{\beta}_{345}^{-1}$ is plotted as a dashed-dotted line. Most of the susceptibility anisotropy comes from the logarithmic term in (42) (it equals 23.0 in weak coupling and 29.7 at the melting pressure). The arrow denotes the position of the transition obtained from Fig. 8.
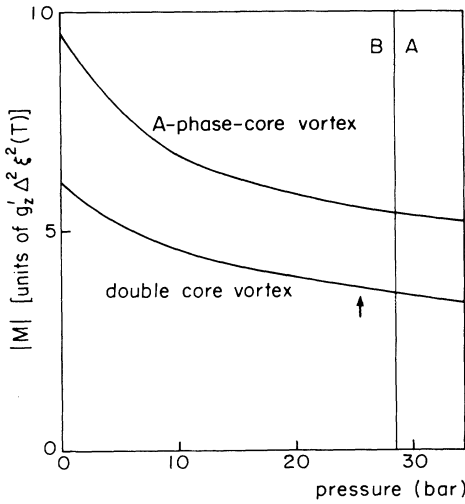
FIG. 11. The magnetic moments of the vortices as a function of pressure in units $g_Z' \Delta^2 \xi^2 (T)$. The moment points in the direction $-R\hat{z}$. The moment of the normal-core vortex is much smaller (< 1) in these units. The arrow denotes the position of the transition.

tion of the symmetry-breaking direction of the double-core vortex and the shift of the vortex-core transition line in magnetic field.

Without the energy terms (5)–(7), the energy of the double-core vortex is completely degenerate in rotations around $\hat{z}$. The dipole forces orient the vortex in zero field so that $\hat{n}$ will be in the x-z plane because $\hat{n}$ in the y direction costs a lot of dipole energy. A high magnetic field orients the vortex such that H will be in the y'-z' plane because the susceptibility in the y' direction is slightly higher than in the x' direction. The characteristic field H_c between the low- and the high-field regions is estimated below. The characteristic field of the bulk B phase is set by the ratio of the coefficients in (5) and (6): $H_c^{\text{bulk}} = (g_D / g_Z)^{1/2} \approx 17$ G (at 18 bars). However, this is modified for vortices because (the anisotropies of) the integrals in (5) and (6) are largely different, the former being logarithmically divergent. The most appropriate cutoff radius for the dipole energy (39) is the dipole length ξ_D. Defining the characteristic field H_c as the field where the anisotropies of (5) and (6) (in the x-y plane) are equal, one gets, from Table II and Fig. 10, $H_c \approx 180$ G at zero pressure, 330 G at 18 bars, and 600 G at the melting pressure. (The latter two are estimates because Table II is evaluated at zero pressure only.) The characteristic fields are evaluated at $T = 0.9 T_c$. The temperature dependence comes from $\xi(T)$ in the logarithmic term (39), which tends to increase H_c at low temperatures. The linear magnetic term (7) is too small to be effective in the orientation at any field. Finally, a highly nonuniform external superflow at the vortex (caused by other vortices in a vortex lattice, for example) could orient the double-core vortex through its anisotropic flow field (Fig. 6) but this effect is not important at the present vortex densities (unit-cell radius $R \approx 100$ μm at 1 rad/s).

The vortex-core transition pressure is shifted in magnet-

ic field because the energies of the vortices are shifted differently due to their different susceptibilities. Estimating $\delta p_v / \delta F \approx 22$ bars/$f_c^B \xi^2(T)$ from Fig. 8 and the susceptibilities from Fig. 10, the shift (at constant T/T_c) is obtained as

$$\delta p_v = (-0.75 H_{x'}^2 - 0.57 H_{y'}^2 + 1.36 H_{z'}^2)$$

$$\times 10^{-6} \frac{1}{1 - T/T_c} \frac{\text{bars}}{\text{G}^2} , \qquad (44)$$

where Table I has been used at 18 bars. For a fixed direction of the vortex and the field, the shift can either be towards lower or higher pressures depending on the $\hat{n}$ vector $[\hat{x}' = \underline{R}(\hat{n}, \theta_0)\hat{x}$, etc.].

VIII. COMPARISON WITH EXPERIMENTS

The different vortices have been observed in a cylindrical cell rotating around its axis (z) characteristically at $\Omega = 1$ rad/s. This corresponds to an equilibrium vortex density $n_v = 2m_3\Omega/\pi\hbar$ and gives $R = 1/(\pi n_v)^{1/2} \approx 100$ μm for the cutoff radius. The vortices were observed because of their effect on $\hat{n}$ and the angle between the magnetic field and $\hat{n}$ was deduced from the NMR frequency shift in most experiments[45] (related techniques were also used). The field was tilted 25° from $\hat{z}$ and its magnitude was 284 or 569 G, the former giving better resolution. Near T_c the NMR signal is so small that it is not possible to measure at temperatures higher than $\approx 0.9 T_c$. The predictions of the GL theory are expected to be fairly accurate at this temperature allowing quantitative comparison between the theory and the experiment.

There is some ambiguity in the comparison of the theory and the experiment because the theoretical results are given as a function of the "Sauls-Serene pressure" which differs from the true pressure. Below (and at the end of the preceding section) the following values were used in calculating the properties of the transition: β parameters at the theoretical (Sauls-Serene) transition pressure and parameters of Table I at 18 bars (real) pressure.

In analyzing the experiments, the effect of the rotation ($\Omega \| \hat{z}$) on the $\hat{n}$ texture was described by two terms,

$$F_Z = \tfrac{2}{5} g_{DZ} \lambda (H \cdot \underline{R} \cdot \hat{z})^2 , \qquad (45a)$$

$$F_Z' = \tfrac{4}{5} g_{DZ} \kappa (H \cdot \underline{R} \cdot \hat{z}) , \qquad (45b)$$

and values for the (Ω-dependent) parameters λ and κ were determined from the observed NMR shift. These are the same energy terms as (6) and (7) and one can thus derive theoretical expressions for λ and κ:

$$\lambda = \frac{5n_v}{4 g_{DZ}} (\chi_{x'x'} \cos\phi_Z + \chi_{y'y'} \sin\phi_Z - \chi_{z'z'}) , \qquad (46a)$$

$$\kappa = -\frac{5n_v}{4 g_{DZ}} M_{z'} . \qquad (46b)$$

The latter is quite obvious but there is a difficulty in the former: (45a) describes the susceptibility difference between the z' direction and the x'-y' plane but there is an anisotropy within the x'-y' plane as well for the double-core vortex. Although the latter anisotropy is relatively

small, it is important to take it into account in a precision calculation of the relative jump of λ in the transition. Expression (45a) can be preserved by introduction of the azimuthal angle ϕ_Z in (46a) that specifies the direction in the x'-y' plane in which the susceptibility is effectively measured in the experiment. In high fields $\phi_Z = 90°$ because the susceptibility is largest in the y direction. At the experimental field, however, the orientation of the double-core vortex is set by the dipole energy and the following approximate procedure may be followed to get ϕ_Z. The magnetic field direction $\hat{H}$ is tilted from $\hat{z}$ by 25° and the angle β between $\hat{n}$ and H can be read from the NMR shift. Because $X_{x'x'} - X_{z'z'} \gg |X_{x'x'} - X_{y'y'}|$, the vectors $\hat{z}$, H, and $\underline{R}^{-1}(\hat{n}, \theta_0)H$ are approximately in the same plane. The dipole energy orients the vortex so that $\hat{n}$ is in the x-z plane. Finally, ϕ_Z is given as the azimuthal angle of the vector $\underline{R}^{-1}H$ in the x-y plane. This is a straightforward geometrical problem and for a typical $\beta = 15°$ one gets $\phi_Z = 16°$,[46] deviating considerably from the high-field result. $\phi_Z = 0$ to a good approximation in (46a).

A second point of concern in the theoretical expression for λ (46a), is the logarithmically divergent susceptibility. The simplest thing is to cut it off at the unit-cell radius R, but there is a better prescription: the normal fluid is in solid-body rotation in the experiment and the velocity determining the asymptotic form (31a) is actually

$$\mathbf{v}_s - \mathbf{v}_n \approx \frac{\hbar}{2m_3}\left[\frac{1}{r} - \frac{r}{R^2}\right]\hat{\phi} \qquad (47)$$

instead of (21). The susceptibility anisotropy is correspondingly reduced and one gets (42), but the logarithm replaced as

$$\ln\left[\frac{R}{\xi(T)}\right] \rightarrow \ln\left[\frac{R}{\xi(T)}\right] - \frac{3}{4}. \qquad (48)$$

The theoretical values of λ are listed in Table III at three different pressures. Their agreement with experiment[47,48] is good: At a fixed pressure one can reasonably extrapolate from the data points at $T \approx 0.9T_c$ to the theoretical value at $T = T_c$. The same applies to the parameter κ (also given in Table III), but the experimental accuracy of κ is much poorer and one can only say that the agreement is much better than by an order of magnitude only.

TABLE III. Theoretical values for the experimentally accessible parameters λ and κ at $\Omega = 1$ rad/s and $T = 0.9T_c$. κ is linear in Ω and independent of T. The same applies to λ, except for an additional dependence coming from the logarithmic term in (42). It is assumed that ϕ_Z in (46a) is zero and the correction (48) is made to (42). The unit of κ is 1 G.

Pressure (bars)	A-phase-core vortex		Double-core vortex	
	λ	κ (G)	λ	κ (G)
34.36	0.15	0.99	0.098	0.64
18	0.30	1.94	0.24	1.31
0	1.66	4.29	1.28	2.75

A direct test of the vortex-core structure is the relative jump of λ at the vortex-core transition. Putting in the numbers as explained above in this section, one gets

$$\frac{\lambda^{A\text{-phase-core}} - \lambda^{\text{double-core}}}{\lambda^{\text{double-core}}} = 0.31 . \qquad (49)$$

This value is valid only at $T = 0.9T_c$ and at the rotation speed of 1 rad/s. The dependence on the temperature and the rotation speed comes from $\xi(T)$ and the cutoff radius R in the logarithmic term (42), the former of which even gives rise to an unphysical divergence at $T = T_c$, but apart from that, the ratio (49) is a constant in the GL theory. (A previously reported estimate (20%) (Ref. 16) for the ratio was obtained neglecting the fine corrections made here [ϕ_Z, Eq. (48), and improved accuracy of Table I].) The experimental value for the relative jump is 0.35 ± 0.05,[48] in agreement with the theory.

The relative jump of κ can be directly read from Fig. 11, giving a 50% jump upwards in the transition from the double-core vortex to the A-phase-core vortex. This jump is in the opposite direction as it is at lower temperatures. At present this prediction cannot reliably be verified due to experimental inaccuracies.

The small differences between the theory and the experiment come from inaccuracies associated with the following (listed approximately in the order of decreasing importance): experiment (especially its extrapolation to T_c), cutoff radius and ϕ_Z for λ, β coefficients, coefficients of Table I, numerical solution of (28), and quasiclassical theory.

The dipole energy (5) was neglected in the analysis of the experiments. Mostly this is justified because it would give a 1% correction to the λ parameter. The whole effect of κ, however, is on the order of the dipole energy, a point that may deserve further study.

The shift of the transition line in magnetic field is calculated in (44) as a function of $\hat{n}$. This gives shifts that should clearly be seen in the experiment if the direction of $\hat{n}$ could be chosen freely. However, essentially no shift of the transition was seen. There is no contradiction between the theory and the experiment because $\underline{R}^{-1}H$ deviates from $\hat{z}$ by an angle 45°–60° in all the experimental runs in the GL region and in those directions the terms in (44) largely cancel each other. At low temperatures ($T \approx 0.8T_c$) the angle is larger, indicating a shift towards lower pressures, and at higher temperatures it is the opposite. This means that, in principle, the transition line at zero magnetic field should be above the measured line (see Fig. 1) at low temperatures and below at high temperatures, although the shift does not exceed the experimental accuracy. This is of interest for the other transition line seen in the hydrodynamic experiment (dashed line in Fig. 1): The magnetic field difference between the NMR and the hydrodynamic experiment does not explain the difference in the transition lines.

The magnetic field also introduces a hysteresis into the transition. There are approximately 600 vortices in the experimental cell and thermodynamically the transition occurs when the configuration with one type of vortex crosses in energy the configuration of the other type.

These configurations have different $\hat{n}$ vectors (because the transition is observed as a change of $\hat{n}$). It is reasonable to expect the real transition to occur when it becomes energetically favorable for one vortex to change its type without essentially changing $\hat{n}$, which is collectively determined by all vortices (if the field is not too high). The hysteresis is explicitly given by (44) because it gives two different shifts depending on either $\hat{n}$ (below or above the transition) to put in. It is not clear which of the hysteretic states is realized in an experiment where the cell is spun up at essentially constant temperature and pressure. This may complicate the precision measurement of the transition line.

Although the GL theory cannot accurately evaluate the latent heat of the vortex-core transition, it should give its order of magnitude. Calculating the entropies from Fig. 8, one can estimate the latent heat at the low-temperature part of the transition line to be $\approx 10^{-6}\,\mu\text{J/mol}$ at 1 rad/s. The latent heat was not studied in the NMR experiment, but it was studied in the hydrodynamic experiment (see Fig. 1). The reported latent heat,[3] however, is 6 orders of magnitude larger than the theoretical and therefore can only be attributed to a misinterpretation of the experiment as discussed in Ref. 49.

A metastable vortex state with a higher-susceptibility anisotropy than that of the equilibrium low-pressure vortex was observed at low temperatures (beyond the GL region).[3] At first sight this fitted well to the picture that the low-pressure vortex has broken rotational symmetry and thus different susceptibility in the x' and y' directions, but there was a difficulty: the magnetic field tends to orient the vortex so that in the equilibrium state the greatest susceptibility is in the direction of the field, implying that the equilibrium state has the highest susceptibility anisotropy ($\chi_{x'x'}, \chi_{y'y'} \gg \chi_{z'z'}$; see Fig. 10). This is just the opposite of the observed behavior. Salomaa and Volovik[17] suggested as a solution that the equilibrium structure of the low-pressure vortex is helical: In the equilibrium the susceptibilities $\chi_{x'x'}$ and $\chi_{y'y'}$ would be effectively averaged, whereas in the transition from the A-phase-core vortex the field could possibly orient the nonhelical metastable state. This marginally gives a qualitative explanation to the observation, but what could cause the helical deformation of the double-core vortex (see the discussion at the end of Sec. V)? In fact, there is a more natural explanation to the problem: At the experimental field of 284 G, the double-core vortex is oriented by the dipole interaction instead of the field, as

shown in the preceding section. It is natural to identify the metastable state as a randomly or magnetic-field-oriented state and the equilibrium state as the dipole-oriented one. Unfortunately the GL theory cannot be used to calculate the NMR shifts at such low temperatures but qualitatively it explains the observed behavior well. The present theory predicts that the metastable-state NMR shift disappears at high fields, where the double-core vortex is oriented by the field.

IX. CONCLUSION

The GL theory of the vortex-core structure in superfluid ^{3}He-B was presented. The theory (having as input only normal-state data in addition to the superfluid transition temperature and no adjustable parameters) gives a transition between two vortices 3 bars below the tricritical pressure, in good agreement with experiment. All the measured properties of the vortices such as the susceptibility anisotropy and the magnetization are well accounted for by the present theory. Although the vortex-core transition (observed by NMR) seems to be conclusively identified, the source of the other transition (observed in critical velocity in powder geometry, Fig. 1) remains open. The determination of $\hat{n}$ texture[44] and the description of the vortex lattice are problems of the hydrodynamic theory (not GL theory) and are therefore not considered here. Nonequilibrium properties were not discussed because they cannot be calculated with the GL theory. Schopohl has recently calculated the excitation spectrum of quasiparticles in the physical vortices using the quasiclassical theory.[50] The full quasiclassical calculation is also needed at low temperatures, where work is in progress.[51] The vortices in the A phase also form a complicated problem that is not studied here, but perhaps the present numerical method could be effective there as well.

ACKNOWLEDGMENTS

[1]P. J. Hakonen, O. T. Ikkala, S. T. Islander, O. V. Lounasmaa, and G. E. Volovik, J. Low Temp. Phys. **53**, 423 (1983).

[2]P. J. Hakonen, M. Krusius, M. M. Salomaa, J. T. Simola, Yu. M. Bunkov, V. P. Mineev, and G. E. Volovik, Phys. Rev. Lett. **51**, 1362 (1983).

[3]J. P. Pekola, J. T. Simola, P. J. Hakonen, M. Krusius, O. V. Lounasmaa, K. K. Nummila, G. Mamniashvili, R. E. Packard, and G. E. Volovik, Phys. Rev. Lett. **53**, 584 (1984).

[4]M. Krusius, P. J. Hakonen, and J. T. Simola, Physica **126B**, 22 (1984).

[5]J. P. Pekola and J. T. Simola, J. Low Temp. Phys. **58**, 555

(1985).

[6]E. V. Thuneberg, Europhys. Lett. **3**, 711 (1987).

[7]T. Ohmi, T. Tsuneto, and T. Fujita, Prog. Theor. Phys. **70**, 647 (1983).

[8]M. M. Salomaa and G. E. Volovik, Phys. Rev. Lett. **51**, 2040 (1983).

[9]M. M. Salomaa and G. E. Volovik, Phys. Rev. B **31**, 203 (1985).

[10]L. D. Landau and E. M. Lifshitz, *Statistical Physics* (Addison-Wesley, Reading, MA, 1969).

[11]T. Passvogel, L. Tewordt, and N. Schopohl, J. Low Temp.

Phys. **56**, 383 (1984).

[12]Y. Hasegawa, Prog. Theor. Phys. **73**, 1258 (1985).

[13]A. L. Fetter and S. Theodorakis, Phys. Rev. Lett. **52**, 2007 (1984).

[14]A. L. Fetter, Phys. Rev. B **31**, 7012 (1985).

[15]J. A. Sauls and J. W. Serene, Phys. Rev. B **32**, 4782 (1985).

[16]E. V. Thuneberg, Phys. Rev. Lett. **56**, 359 (1986).

[17]M. M. Salomaa and G. E. Volovik, Phys. Rev. Lett. **56**, 363 (1986).

[18]A. L. Fetter, Phys. Rev. Lett. **57**, 2092 (1982).

[19]H. Smith, W. F. Brinkman, and S. Engelsberg, Phys. Rev. B **15**, 199 (1977).

[20]A. L. Fetter, in *Progress in Low Temperature Physics,* edited by D. F. Brewer (North-Holland, Amsterdam, 1986), Vol. 10.

[21]V. P. Mineev, M. M. Salomaa, and O. V. Lounasmaa, Nature (London) **324**, 333 (1986). The interpretation of the double-core vortex given in Fig. 8 of this reference does not satisfy, among other things, the symmetries of the vortex.

[22]A. L. Fetter, Can. J. Phys. (to be published).

[23]J. W. Serene and D. Rainer, Phys. Rep. **101**, 221 (1983).

[24]D. Vollhardt, K. Maki, and N. Schopohl, J. Low Temp. Phys. **39**, 79 (1980).

[25]D. S. Greywall, Phys. Rev. B **33**, 7520 (1986).

[26]J. C. Wheatley, Rev. Mod. Phys. **47**, 415 (1975).

[27]J. A. Sauls and J. W. Serene, Phys. Rev. B **24**, 183 (1981).

[28]A. I. Ahonen, M. Krusius, and M. A. Paalanen, J. Low Temp. Phys. **25**, 421 (1976).

[29]G. F. Spencer, P. W. Alexander, and G. G. Ihas, Physica **107B**, 289 (1981).

[30]D. C. Sagan, P. G. N. deVegvar, E. Polturak, L. Friedman, S.-S. Yan, E. L. Ziercher, and D. M. Lee, Phys. Rev. Lett. **53**, 1939 (1984).

[31]U. E. Israelsson, B. C. Crooker, H. M. Bozler, and C. M. Gould, Phys. Rev. Lett. **53**, 1943 (1984).

[32]N. D. Mermin and G. Stare, Phys. Rev. Lett. **30**, 1135 (1973).

[33]L. J. Buchholtz and A. L. Fetter, Phys. Rev. B **15**, 5225 (1977).

[34]J. W. Serene and D. Rainer, Phys. Rev. B **17**, 2901 (1978).

[35]The estimate for Ω by M. M. Salomaa and G. E. Volovik, Phys. Rev. Lett. **52**, 2008 (1984), is too small by 3 orders of magnitude at least.

[36]L. D. Landau and E. M. Lifshitz, *Quantum Mechanics* (Pergamon, London, 1958).

[37]E. V. Thuneberg, Phys. Rev. Lett. **57**, 2093 (1986).

[38]V. P. Mineev and M. M. Salomaa, J. Phys. C **17**, L181 (1984).

[39]D. Rainer and M. Vuorio, J. Phys. C **10**, 3093 (1977).

[40]R. Kaul and H. Kleinert, J. Low Temp. Phys. **38**, 539 (1980).

[41]N. Schopohl (unpublished).

[42]M. Abramowitz and I. A. Stegun, *Handbook of Mathematical Functions* (Dover, New York, 1970).

[43]S. L. Adler and T. Piran, Rev. Mod. Phys. **56**, 1 (1984).

[44]E. B. Sonin, J. Low Temp. Phys. **55**, 533 (1984).

[45]Yu. M. Bunkov, P. J. Hakonen and M. Krusius, in *Quantum Fluids and Solids—1983 (Sanibel Island, Fla.),* AIP Conf. Proc. No. 103, edited by E. D. Adams and G. G. Ihas (AIP, New York, 1983), p. 194.

[46]$\phi_Z = \arccos\{\cos(\beta)/[1 - 5\sin^2(\beta)/8]^{1/2}\}/\sin(\mu+\nu/2)$, where $\nu = \arccos[1 - 5\sin^2(\beta)/4]$ and β is the angle between $\hat{n}$ and $\mathbf{H}$ and μ the angle between $\hat{z}$ and $\mathbf{H}$.

[47]P. J. Hakonen, M. Krusius, G. Mamniashvili, and J. T. Simola, in *Proceedings of the 17th International Conference on Low Temperature Physics (LT-17),* edited by U. Eckern, A. Schmid, W. Weber, and H. Wühl (North-Holland, Amsterdam, 1984), p. 1366.

[48]P. J. Hakonen (private communication).

[49]E. V. Thuneberg, Phys. Rev. B **33**, 5124 (1986).

[50]N. Schopohl (unpublished).

[51]N. Schopohl and E. V. Thuneberg (unpublished).